Acta Geochim (2025) 44:962–978
https://doi.org/10.1007/s11631-025-00766-x

ORIGINAL ARTICLE

Geochemistry and mineralogy of ilmenite exsolutions in titanomagnetite and their implications for the ore-forming process at the Damiao deposit

Kaiyuan Wang[1] · Hongtao He[1] · Wenjie Shi[1]

Received: 24 January 2025 / Revised: 30 January 2025 / Accepted: 3 February 2025 / Published online: 24 February 2025

Abstract The Damiao Fe-Ti-P deposit, located within the Damiao anorthosite complex in northeastern China, features Fe-Ti oxide ores and nelsonites that occur as irregularly inclined stratiform-like bodies, lenses, or veins with sharp contacts against anorthosite and gabbronorite. This deposit is characterized by abundant titanomagnetite that hosts diverse ilmenite exsolution textures, including blocky, lamellar, and cloth-like forms. In this study, we investigate the geochemistry and mineralogy of ilmenite exsolutions in titanomagnetite to understand their formation mechanisms and implications for the ore-forming process. Detailed petrographic observations and electron microprobe analyses reveal that the exsolution textures result from multiple mechanisms: oxy-exsolution due to titanomagnetite oxidation; subsolidus re-equilibration between magnetite and ilmenite involving elemental diffusion of Fe, Ti, Cr, Co, and Ni; and exsolution related to lattice defects caused by rapid cooling. Thermodynamic modeling using Gibbs free energy calculations, and the QUILF program indicates that blocky, lamellar, and cloth-textured ilmenite exsolutions formed at temperatures above and below the solid-solution solvus under decreasing oxygen fugacity. Additionally, our results indicate that the exsolution of zircon and pleonaste at ilmenite grain boundaries is attributed to the saturation and precipitation of elements like Zr and Al, due to the oxidation of titanomagnetite, rather than interactions between ilmenite and adjacent clinopyroxene. Reconstruction of the cooling history suggests that the oxygen fugacity of oxide–apatite gabbronorites was significantly higher than that of Fe-Ti-P ores. This confirms that increasing oxygen fugacity during magma evolution promoted immiscibility, leading to the formation of nelsonitic melts and ultimately the development of Fe-Ti-P ores.

Keywords Ilmenite exsolution · Oxy-exsolution · Titanomagnetite · Subsolidus re-equilibration · Damiao Fe-Ti-P deposit

1 Introduction

Magmatic Fe-Ti oxide deposits are significant sources of iron, titanium, vanadium, and phosphorus, commonly associated with mafic–ultramafic intrusions and Proterozoic anorthosite complexes. Recent studies indicate that these deposits are also related to late-stage crustal tectonic activities and associated hydrothermal processes (Buelens et al. 2024; Liu et al. 2024; Khedr et al. 2024). The Damiao deposit stands out due to its rich occurrence of titanomagnetite with complex ilmenite exsolution textures. This setting allows for an in-depth study of magmatic differentiation, cooling rates, and post-magmatic processes such as hydrothermal alteration. The diversity of ilmenite exsolution textures indicates varying physicochemical conditions during and after crystallization, providing insights into the ore-forming mechanisms of Fe-Ti oxide deposits (Wei et al. 2020; Li et al. 2019a, b).

Supplementary Information The online version contains supplementary material available at https://doi.org/10.1007/s11631-025-00766-x.

✉ Kaiyuan Wang
wangkaiyuan@hebeu.edu.cn

Hongtao He
hehongtao@hebeu.edu.cn

Wenjie Shi
1739887013@qq.com

[1] School of Earth Science and Engineering, Hebei University of Engineering, Taiji Road, Handan 056038, Hebei, China

Understanding the formation mechanisms of these exsolutions is crucial for unraveling the redox state and geochemical evolution of the magma, and ore-forming processes (Pochon et al. 2024).

Titanomagnetite, a solid solution of magnetite (Fe_3O_4) and ulvöspinel (Fe_2TiO_4), crystallizes from Fe-Ti–rich magmas under varying temperature, oxygen fugacity, melt composition, and cooling rate (Gennaro et al. 2024; Kehdr et al. 2024). Upon cooling, titanomagnetite often undergoes subsolidus exsolution, resulting in the precipitation of ilmenite ($FeTiO_3$) and other oxide phases. The textures and compositions of exsolved minerals reveal physicochemical conditions during and after crystallization. Advanced techniques like atom probe tomography offer higher resolution and reveal titanomagnetite–ilmenite interactions at the lattice scale (Dellefant et al. 2024).

Several mechanisms have been proposed for the formation of ilmenite exsolutions in titanomagnetite, including the oxyexsolution of ulvöspinel, subsolidus re-equilibration between magnetite and ilmenite, and cation-deficient mechanisms linked to rapid cooling and lattice defects. Recent high-resolution microstructural analyses indicate that the formation of ilmenite exsolutions may also involve complex multistage redox reactions (Frost 1991; Tan et al. 2016; Gao et al. 2019; Arguin et al. 2018; Miloski et al. 2024). Despite extensive studies, the precise mechanisms responsible for ilmenite exsolution and their relative contributions, such as the exact role of oxygen fugacity, temperature, volatile content (e.g., fluorine, chlorine), and the relative proportion of oxide minerals, remain subjects of debate. Furthermore, these mechanisms offer pathways to explore broader scientific issues, such as the kinetic factors influencing mineral transformations and the temporal evolution of magmatic systems.

In the Damiao deposit, previous research has documented the presence of various ilmenite exsolution textures within titanomagnetite, including blocky, lamellar, cloth-like, acicular, granular, and structures with complex multistage growth rims, which are believed to result from distinct physicochemical conditions (Wei et al. 2020; Li et al. 2019a, b, 2024a, b). However, a comprehensive geochemical and mineralogical analysis of these exsolutions is lacking. Such an investigation is important for interpreting the cooling history of the Fe-Ti-P oxide rocks and assessing the implications for the ore-forming processes.

In this study, we examine the geochemistry and mineralogy of ilmenite exsolutions in titanomagnetite from the Damiao deposit. By analyzing the compositions and textures of these exsolutions using techniques such as in situ analysis, compositional mapping, and thermodynamic modeling, we aim to better understand their formation mechanisms and the specific conditions, such as temperature and oxygen fugacity, under which they formed. Additionally, we discuss the implications of our findings for the cooling history of the Damiao Fe-Ti-P oxide rocks and the ore-forming processes involved.

2 Geological background

The North China Craton, a significant Archean to Paleoproterozoic geological entity, was formed through the amalgamation of the Eastern and Western Blocks along the Trans-North China Orogen (TNCO) around 1.85 Ga (Yan et al. 2025; Wan et al. 2013; Fig. 1a). This orogenic belt served as the suture zone where the two blocks collided and stabilized to create the craton. The basement rocks of the craton consist predominantly of high-grade metamorphic assemblages, including granitic migmatites, gneisses, schists, and marbles, overlain by Mesoproterozoic to Cenozoic sedimentary sequences (Li et al. 2024a, b; He et al. 2016).

Located in the northern part of the TNCO, the Damiao anorthosite complex is a prominent Proterozoic intrusion emplaced approximately 1.74 Ga during a post-collisional tectonic setting (Chen et al. 2013; He et al. 2016; Fig. 1b). This complex is part of the Anorthosite–Mangerite–Charnockite–Granite suite, associated with rapakivi granites. It reflects significant crustal differentiation events during the late Paleoproterozoic (Yang et al. 2014; Liu et al. 2016). The Damiao complex intruded Neoarchean high-grade metamorphic rocks of the Dantazi Group, dated at around 2.5 Ga. It is unconformably overlain by Jurassic volcanic and sedimentary rocks (Li et al. 2019a, b; Zhai and Santosh 2013).

The Damiao anorthosite complex is divided into three distinct bodies: the Eastern, Central, and Western Bodies (Zhao et al. 2009; Li et al. 2019a, b; Fig. 1b). The Western Body, being the largest with an area of approximately 80 km^2, comprises extensive volumes of anorthosite along with minor occurrences of leuconorite, oxide–apatite gabbronorite, mangerite, and significant Fe-Ti-P orebodies (He et al. 2016, 2019; Zhao et al. 2009). Deep drilling beneath the Western Body has revealed a substantial olivine–titanomagnetite-rich layered intrusion, suggesting the presence of mafic residues from the differentiation of a high-aluminum basaltic parental magma (He et al. 2016, 2019; Zhao et al. 2009).

Magmatic activity within the Damiao complex is characterized by two main stages. The early stage involved the emplacement of anorthosite with minor norite components, while the late stage introduced mangerite and Fe-Ti-P-rich dikes and veins that intruded the existing anorthosite massif (Wang et al. 2017; Li et al. 2014, 2019a, b). The early-stage anorthosite exhibits two facies based on coloration: a dark-colored, relatively unaltered variety, and a light-colored, extensively altered type (Wei et al. 2020). The dark-colored anorthosite primarily consists of plagioclase (An_{40-55}) and subordinate amounts of pyroxenes (hypersthene and

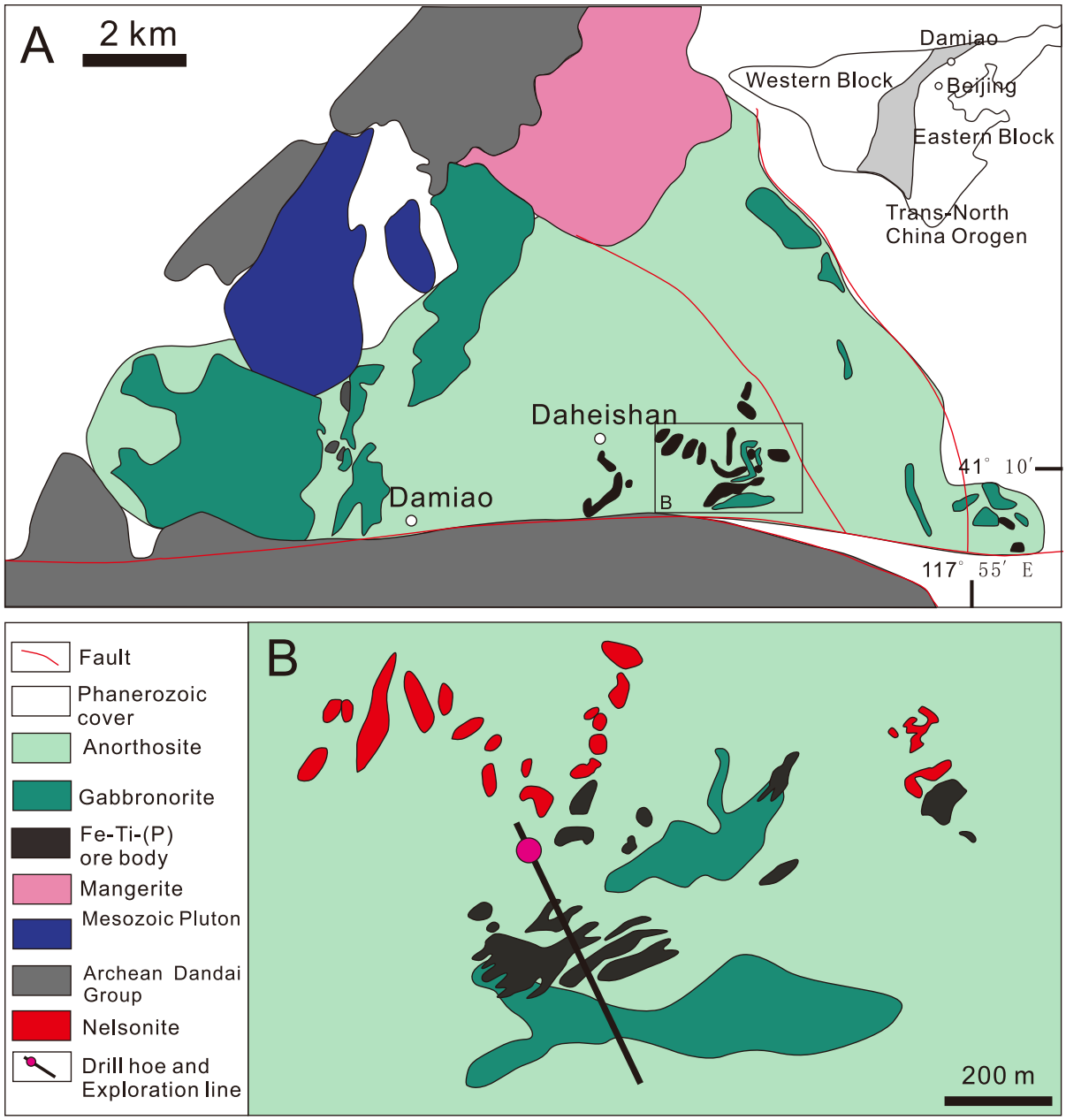

Fig. 1 **a**. Geological map of the Damiao anorthosite complex; **b**. lensoidal, irregularly-shaped veins of nelsonite and Fe-Ti oxide ores intruding into the anorthosite and gabbronorite (Revised from He et al. 2016)

diopside) and Fe-Ti oxides. In contrast, the light-colored anorthosite has undergone hydrothermal alteration, with plagioclase transformed into albite and clinozoisite and pyroxenes replaced by chlorite and magnetite (Teng et al. 2015; Li et al. 2014, 2019a, b).

Fe-Ti-P-rich rocks in the Damiao complex occur as dikes and veins with irregular yet sharp contacts, cross-cutting the earlier anorthosite units. These rocks include oxide–apatite gabbronorite, Fe-Ti-P-rich pyroxenite, and massive Fe-Ti-(P) orebodies (Chen et al. 2013; He et al. 2016, 2019; Fig. 1). The orebodies are predominantly lens-shaped or form steeply inclined stratiform bodies within the anorthosite and leuconorite, displaying various sizes that can reach up to tens of meters in width and hundreds of meters in length. Mineralogical zoning within these orebodies is common, with apatite-rich zones near the tops and margins and oxide-rich zones toward the centers and bases, indicating possible gravitational differentiation during crystallization (Zhao et al. 2009; Li et al. 2014, 2019a, b).

The complex also hosts minor occurrences of mangerite, particularly in the northwestern region of the Western Body, which is considered a late-stage differentiative product of the parental magma. Additionally, ferrodioritic, gabbroic, and felsic dykes are present, suggesting multiple intrusive events and a prolonged magmatic history (Chen et al. 2013; He et al. 2016, 2019).

3 Analytical methods

3.1 Whole-rock major element analysis

Bulk rock samples were crushed and pulverized to a fine powder for whole-rock geochemical analysis. Major elements were determined by X-ray fluorescence (XRF) spectrometry using a Rigaku ZSX Primus II XRF instrument at the ALS Laboratory Group. Fused glass beads were prepared from the powdered samples using a lithium tetraborate flux. Calibration was performed using certified reference materials GSR-1–GSR-6 issued by the Chinese National Standards. Analytical precision and accuracy were monitored by repeated analyses of standard reference materials and duplicates, with relative standard deviations better than 2% for most major elements. Trace element geochemistry was analyzed by ICP-MS at the Institute of Geochemistry, Guiyang (Chinese Academy of Sciences; GIGCAS). Detailed analytical methodology was outlined in Qi and Zhou (2008).

3.2 Electron probe microanalysis (EPMA)

Mineral compositions of magnetite, ilmenite, clinopyroxene, and apatite were determined using a JEOL JXA-8230 electron probe microanalyzer (EPMA) at the GIGCAS. Backscattered electron (BSE) imaging was employed to identify exsolution textures and select suitable areas for analysis. The analytical conditions were optimized to obtain accurate major element concentrations: an accelerating voltage of 15 kV, a beam current of 20 nA, and a focused beam diameter of 1 μm. Natural and synthetic standards were used for calibration, including Fe_2O_3 for iron, TiO_2 for titanium, Cr_2O_3 for chromium, $MnTiO_3$ for manganese, and NiO for nickel. Matrix corrections were applied using the ZAF method. Detection limits for most elements were below 0.01 wt%. To avoid beam damage and element migration, particularly for alkali elements in apatite, a defocused beam (5 μm) was used when necessary.

3.3 Laser ablation inductively coupled plasma mass spectrometry

Trace element concentrations in magnetite, ilmenite, plagioclase, and apatite were measured by LA-ICP-MS at the GIGCAS. An Agilent 7900 ICP-MS instrument was coupled with a resolution SE 193 nm ArF excimer laser ablation system equipped with a two-volume S-155 ablation cell (Australian Scientific Instruments). The laser spot sizes were 44 μm for apatite and plagioclase, and 60 μm for magnetite and ilmenite, with a repetition rate of 6 Hz and energy density of ~3.5 J/cm^2. Helium was used as the carrier gas to transport the ablated aerosol to the ICP-MS, with argon make-up gas introduced before the plasma. Calibration was performed using NIST SRM 610 as the external standard and ^{57}Fe or ^{43}Ca as internal standards for magnetite/ilmenite and apatite/plagioclase, respectively. Repetition of analyses on standard reference materials BCR-2G, BHVO-2G, and BIR-1G served to monitor accuracy and precision, yielding results within 5% of recommended values. Data reduction was carried out using the software Iolite, following the protocols described by Paton et al. (2011). Special attention was given to exclude inclusions and surface contamination by examining time-resolved spectra; signals with irregularities were discarded. Detection limits for trace elements were typically in the range of 0.01–0.1 ppm.

4 Results

4.1 Mineral chemistry of magnetite, ilmenite, and pleonaste

The magnetite in the Damiao Fe-Ti-P deposit exhibits a relatively narrow range of compositions. Most magnetite samples have Fe_3O_4 content exceeding 90%, with TiO_2 and Al_2O_3 contents both below 1%. Trace elements in magnetite exhibit considerable variability, with concentrations of siderophile elements such as Cr, Co, Ni, Ti, and Zn reaching up to 0.5%. The positive correlations between FeO and TiO_2 and Al_2O_3 indicate that these elements are incorporated into the crystal lattices of magnetite and ilmenite during crystallization (Fig. 7).

Granular ilmenite exhibits Fe_2O_3 contents ranging from 5 to 25%, with almost no pure $FeTiO_3$ present. MnO content fluctuates around 1%. In addition to Fe and Ti, ilmenite contains significant trace elements, with relatively high concentrations of Zn and V. The composition of exsolved ilmenite lamellae in titanomagnetite is similar to that of granular ilmenite. Pleonaste is mainly distributed at the interface between magnetite and exsolved ilmenite, with primary components including Al_2O_3, FeO, and TiO_2 (Fig. 7).

4.2 Exsolution textures in titanomagnetite

The exsolution textures of ilmenite in titanomagnetite show significant diversity, including blocky, lamellar, and

cloth-like textures, indicating complex thermal histories and crystallization processes.

Blocky exsolutions: Blocky exsolutions of ilmenite mainly appear as thick lamellae aligned along multiple {111} planes of the magnetite crystal lattice, forming a grid-like pattern. These lamellae, tens to hundreds of microns thick, indicate formation under high-temperature conditions. Blocky exsolutions are typically observed in the core areas of titanomagnetite grains, reflecting the initial high-temperature exsolution process (Figs. 2 and 3).

Lamellar exsolutions: Lamellar exsolutions of ilmenite are predominantly aligned along a single set of {111} planes, usually with a thickness exceeding 100 microns. This texture suggests significant growth under prolonged high-temperature conditions, indicating that ilmenite underwent an exsolution process during high-temperature conditions (Figs. 5 and 6).

Cloth-Like exsolutions: Cloth-like exsolutions primarily include fabric-like textures, thin lamellae, and mottled vermicular intergrowths. Fabric-like textures are characterized by minute ilmenite intergrowths dispersed throughout the magnetite matrix, resembling woven fabric patterns, indicative of the initial oxidation stage of titanomagnetite at lower temperatures. Thin lamellae are aligned along {111} planes with a thickness ranging from 1 to 5 microns. Mottled and vermicular intergrowths typically occur near grain boundaries and fractures, varying in size from a few microns to several tens of microns, indicating advanced stages of ilmenite exsolution during diffusion (Figs. 5 and 6).

Additionally, there are exsolutions of pleonaste and zircon within ilmenite. Zircon exsolutions are primarily distributed at grain boundaries as minute inclusions, which are typically aligned along fractures or interfaces between the ilmenite and other minerals, such as clinopyroxene (Fig. 4).

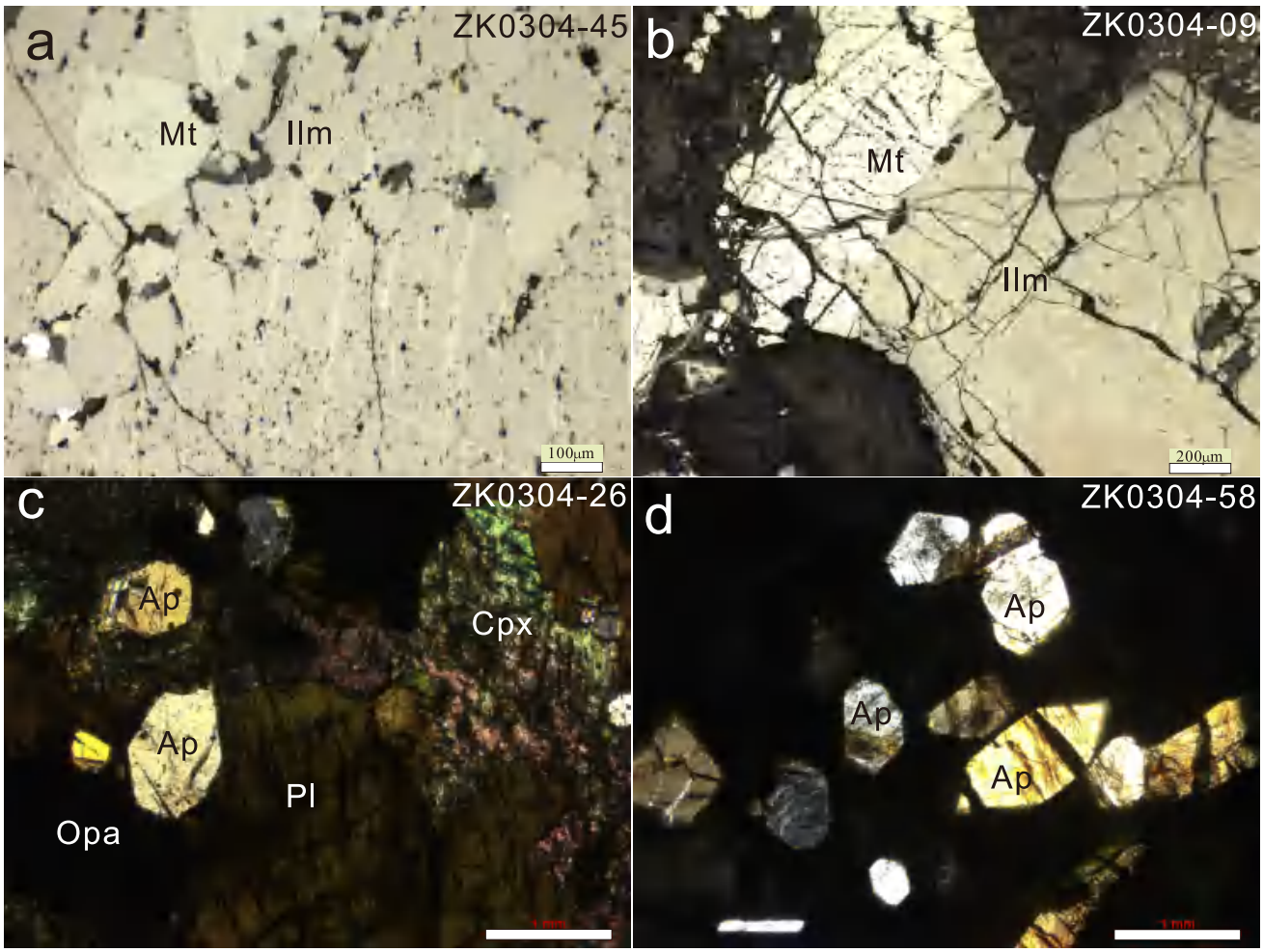

Fig. 2 Photomicrographs of the Damiao Rocks and Ores. **a**. Massive Fe-Ti Ore: Coarse-grained euhedral magnetite and ilmenite with sharp boundaries. **b**. Nelsonite: Euhedral magnetite, ilmenite, and euhedral to subhedral apatite making up to 90% of the rock. **c**. Gabbronorite: Plagioclase, oxides, and euhedral to subhedral apatite. **d**. Gabbro-Nelsonite: Interstitial anhedral plagioclase among Fe-Ti oxides and euhedral to subhedral apatite

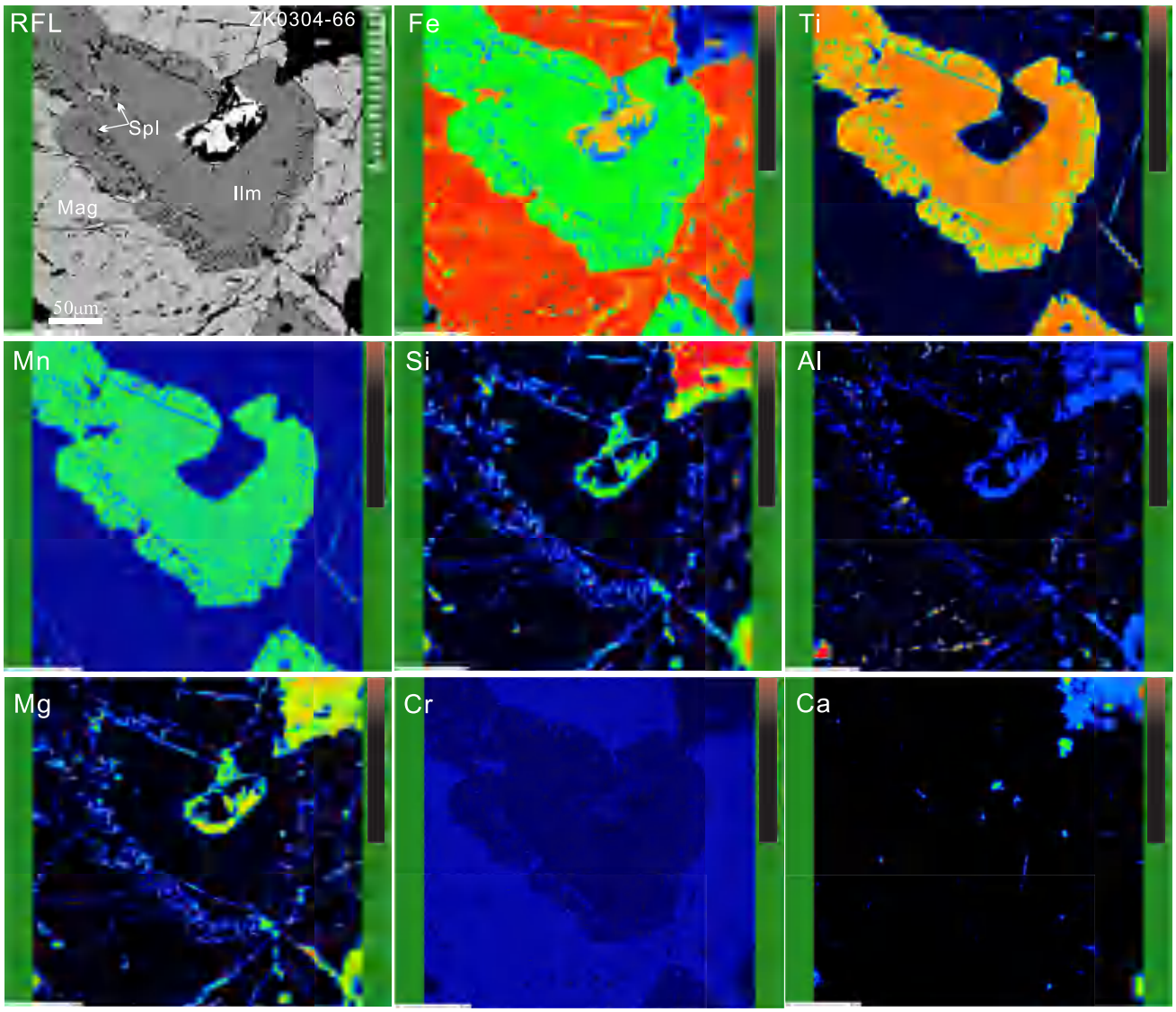

Fig. 3 EPMA element map of the exsolved ilmenite and titanomagnetite in Fe-Ti Ore from the Damiao deposit, which illustrates the distribution of various major elements between the mineral phases. The relative concentrations of the elements are semiquantitative. Granule and thick ilmenite lamellae and pleonaste particles in the host magnetite. Pleonaste is distributed around the edges of the ilmenite

5 Discussion

5.1 Formation of ilmenite exsolution textures in magnetite-ulvöspinel solid solution

In iron-rich, titanium–phosphorus magmas, the crystallization of minerals such as magnetite, ilmenite, apatite, and rutile reflects the evolution of magma temperature, oxygen fugacity, and composition (Bhattacharjee and Mondal 2021; Tan et al. 2016, 2021). Currently, three potential mechanisms have been proposed for the formation of exsolved ilmenite: oxy-exsolution of titanomagnetite; inter-oxide re-equilibration between magnetite and ilmenite; and the formation of ilmenite due to cation deficiency caused by rapid cooling of magma leading to lattice defects (Arguin et al. 2018; Wei et al. 2020). Magnetite–ulvöspinel solid solutions can transform into ilmenite under oxidizing conditions, and the composition and structure of the resulting ilmenite vary depending on temperature, oxygen fugacity, and the composition of the solid solution (Lusted 2019; Gorbatova et al. 2021). Therefore, the blocky, lamellar, and cloth-textured ilmenite exsolutions observed in the Damiao magnetite deposit are likely formed during different stages of Fe-Ti-P magmatic evolution (Figs. 5 and 6). The solvus temperature of magnetite–ulvöspinel solid solutions fluctuates with changes in chemical composition, peaking at approximately 450–600 °C (Otto 2017; Arguin et al. 2018). while the solvus temperature based on the relative content of magnetite and

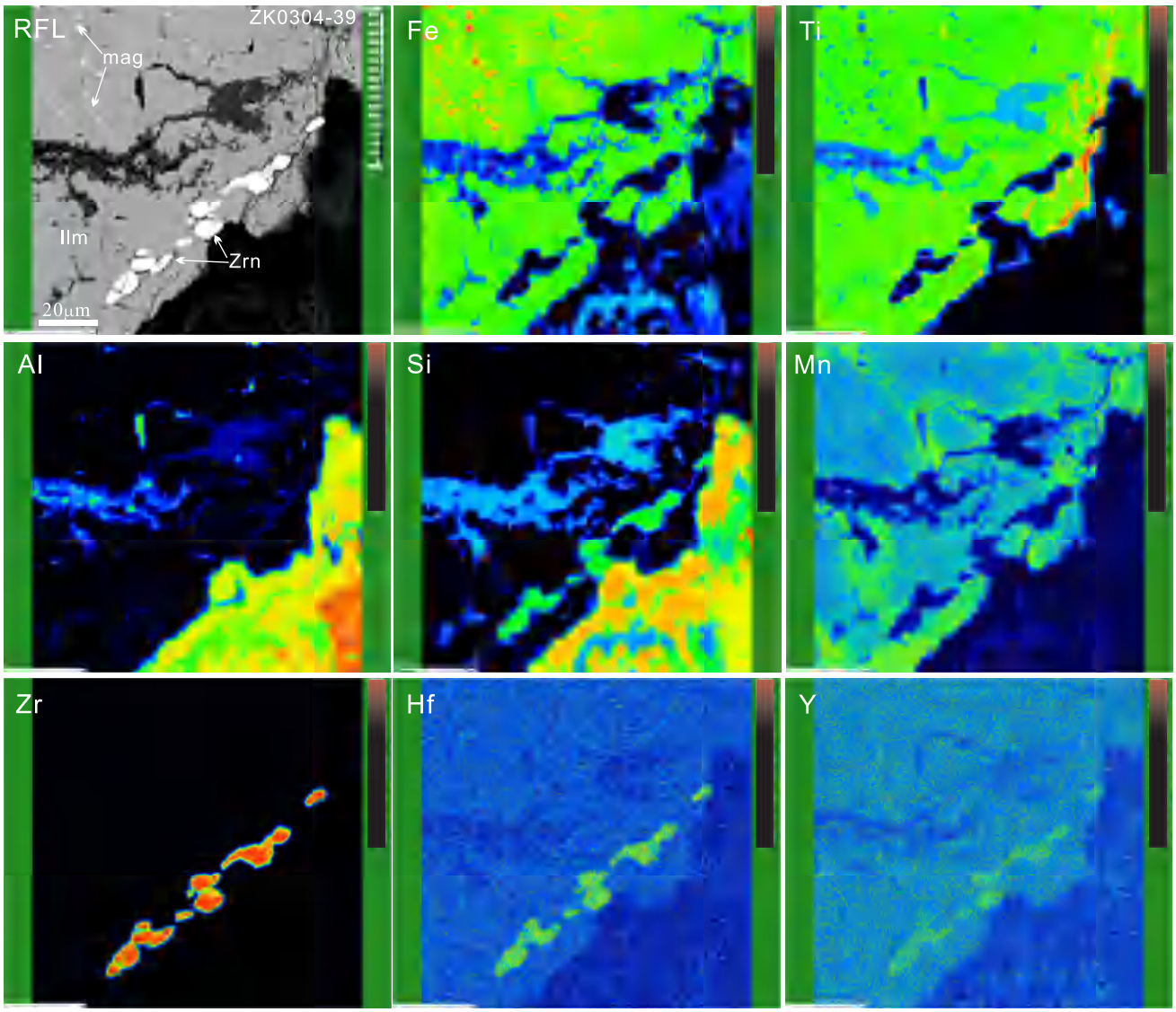

Fig. 4 EPMA element map of ilmenite in Fe-Ti Ore from the Damiao deposit. There is the appearance of fine-grained magnetite exsolution within the ilmenite, while zircon is distributed around the edges of ilmenite

ulvöspinel in the Damiao deposit is around 450 °C. The similar spatial distribution and chemical composition among the various textural types of ilmenite exsolutions in the Damiao deposit suggest that the textural diversity is primarily the result of multiple oxidation reactions occurring in compositionally uniform Fe-Ti-P magma under varying temperature conditions (Figs. 5 and 6). Calculations of temperature and oxygen fugacity for magnetite-ilmenite pairs indicate that blocky and lamellar ilmenite exsolutions formed above the solvus temperature, around 620 °C, whereas cloth-textured ilmenite exsolutions formed below the solvus temperature of around 450 °C. Therefore, the similar compositions and narrow compositional range of magnetite–ulvöspinel in different structures at Damiao confirm that the theories attributing the diversity of iron–titanium oxide structures to multiple magma replenishments or assimilation and contamination of wall rocks are unreasonable (Lee et al. 2022; Khedr et al. 2024).

$$6Fe_2TiO_4 + O_2 = 6FeTiO_3 + 2Fe_3O_4 \quad (1)$$

Experimental studies have demonstrated that magnetite–ulvöspinel solid solutions can produce various types of ilmenite exsolutions through vacancy relaxation mechanisms under high temperatures (> 900 °C) and anoxic reducing conditions (Pearce et al. 2010; Lilova et al. 2012). In this process, Fe^{2+} ions replace high-valence ions such as Ti^{4+} and Cr^{3+} in adjacent ilmenite, leading to lattice defects (Noh et al. 2015; Özdemir and Dunlop 1997). This mechanism

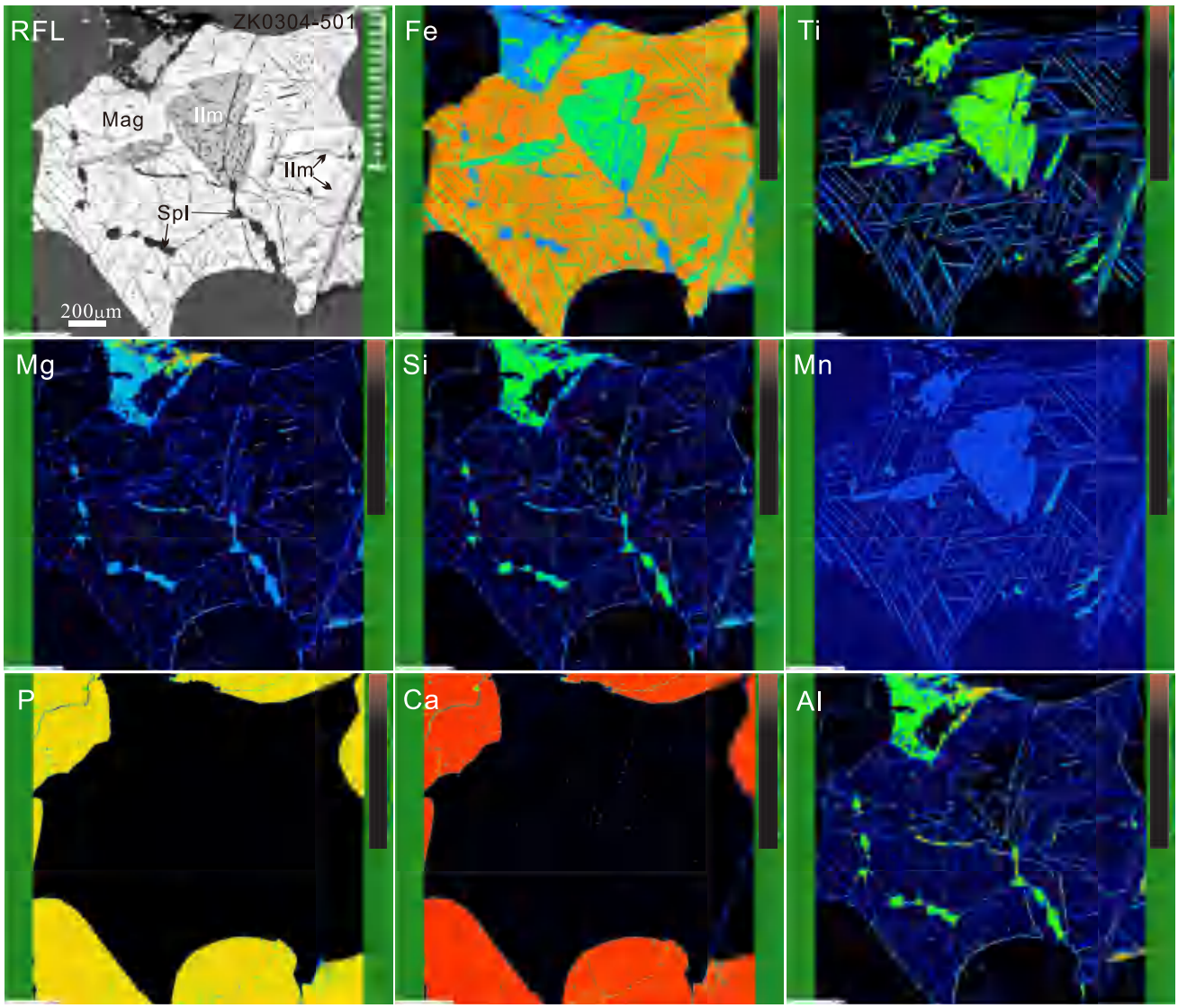

Fig. 5 EPMA element map of the exsolved ilmenite and titanomagnetite in Fe-Ti Ore from the Damiao deposit, blotchy ilmenite exsolution is observed in the central region of titanomagnetite. This blotchy ilmenite exhibits both hexagonal and pyramidal shapes with threefold rotational symmetry, which is consistent with the crystal structure of magnetite along the *c*-axis, indicating that the (0001) plane of ilmenite is parallel to the (111) plane of magnetite. Additionally, lamellar ilmenite exsolution appears in titanomagnetite along the (110) plane direction of the magnetite

effectively explains the exsolution textures of iron–titanium oxides in mantle xenoliths (Lattard 1995). However, both our thermodynamic simulations and geochemical experiments have confirmed that, as the Damiao magma evolves, the temperature and oxygen fugacity gradually decrease, which closely aligns with the isopleths of Fe-Ti oxide solid solutions containing about 30% ulvöspinel content. Consequently, the probability of lattice defect formation decreases significantly (Lattard 1995). Therefore, this mechanism cannot be considered the primary cause of ilmenite exsolution textures in igneous or metamorphic rocks. Based on subsolidus re-equilibration reactions between magnetite and ilmenite, as well as the oxidation reactions of titanomagnetite, the formation temperature of ilmenite exsolution textures in the Damiao deposit is approximately 550–680 °C. These conditions do not align with those required for lattice defect-induced ilmenite exsolution.

Both the oxidation of titanomagnetite and the re-equilibration reactions between magnetite and ilmenite involve the rearrangement of cations and a transformation of the oxygen sublattice from a face-centered cubic to a hexagonal close-packed framework (Gruenewaldt et al. 1995; Arguin et al. 2018). Previous solution–precipitation experiments investigating heterogeneous nucleation and crystal growth

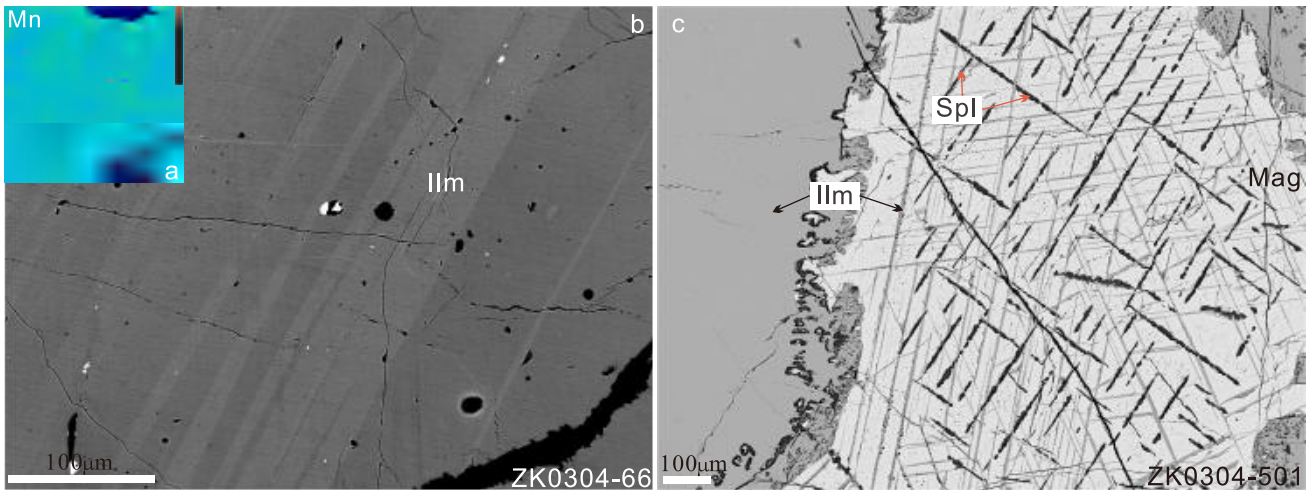

Fig. 6 **a** Backscattered images show the presence of a striped structure within the ilmenite, which has a weak correlation with the Mn element mapping results, but no correlation with the other element mapping results; **b** Lamellae of pleonaste lying on the (100) planes of the magnetite; the presence of a fine pattern of ulvöspinel micro-intergrowths on the same plane of the host and the crosscutting relationship with pleonaste should also be noted

processes have found that, during transformations between different crystal configurations, the crystallographic orientation of newly formed crystals is nearly parallel or slightly inclined to that of the substrate crystals (Watanabe and Funakubo 2006; Carter and Ward 1993). This orientation accommodates lattice misfits or dislocations and accounts for differences in surface energy between the two minerals. The blocky or cloth-textured ilmenite crystals exsolved in Damiao magnetite formed during different stages of solid-solution evolution, yet they all crystallized along the < 111 > crystallographic axes (Fig. 5). Remarkably, the blocky ilmenite exhibits both hexagonal and pyramidal shapes with threefold rotational symmetry, consistent with the *c*-axis orientation of magnetite crystals. This observation indicates that the (0001) basal plane of ilmenite remains parallel to the (111) plane of magnetite (Fig. 5). Tan et al. (2021) also observed consistent crystallographic orientations in magnetite–ilmenite–rutile symplectites within the Panzhihua intrusion. Therefore, the crystallographic orientation and morphological characteristics of exsolved ilmenite crystals are largely controlled by the crystalline substrate of titanomagnetite.

5.2 Subsolidus re-equilibration mechanisms of iron–titanium oxides

Under subsolidus temperature conditions, elemental re-equilibration reactions within iron–titanium oxides can alter the chemical compositions of magnetite and ilmenite and may lead to the exsolution of ilmenite within magnetite (Adak et al. 2021; Wei et al. 2020). In the Damiao deposit, the Fe^{3+} proportions, V/Sc and Cr/Fe ratios in magnetite–ulvöspinel and ilmenite–hematite solid solutions evolved almost synchronously (Fig. 7). This synchronicity suggests that these solid solutions share similar crystallization and compositional evolution histories in the Fe-Ti-P magma. The fluctuations in the V/Sc ratio indicate changes in oxygen fugacity during magma evolution, as V and Sc have similar atomic radii but different valence states (+3 for Sc and multiple valence states for V). The Ni/Cr ratios in iron oxides decrease uniformly and gradually with magma evolution, indicating minimal influence of sulfides on the chemical compositions of iron oxides. This observation aligns with the geological fact of low sulfide content in the Damiao deposit. Collectively, these facts suggest a high likelihood of subsolidus elemental diffusion reactions among iron oxides in the Damiao deposit.

Elemental diffusion, particularly that which conforms to valence and stoichiometric balance, provides a plausible explanation for the exsolution of ilmenite within magnetite (Tan et al. 2016, 2019; Arguin et al. 2018). Under subsolidus conditions, magnetite–ulvöspinel and ilmenite–hematite solid solutions can undergo Fe and Ti ionic re-equilibration reactions, specifically:

$$Fe^{2+} + Ti^{4+} = 2Fe^{3+} \tag{2}$$

The specific chemical equation is:

$$Fe_2TiO_4\left(\text{in Usp} - Mt_{ss}\right) + Fe_2O_3\left(\text{in Hem} - Ilm_{ss}\right) = FeTiO_3\left(\text{in Hem} - Ilm_{ss}\right) + Fe_3O_4\left(\text{in Usp} - Mt_{ss}\right) \tag{3}$$

As the temperature decreases, this reaction progressively advances toward the right, favoring the formation of

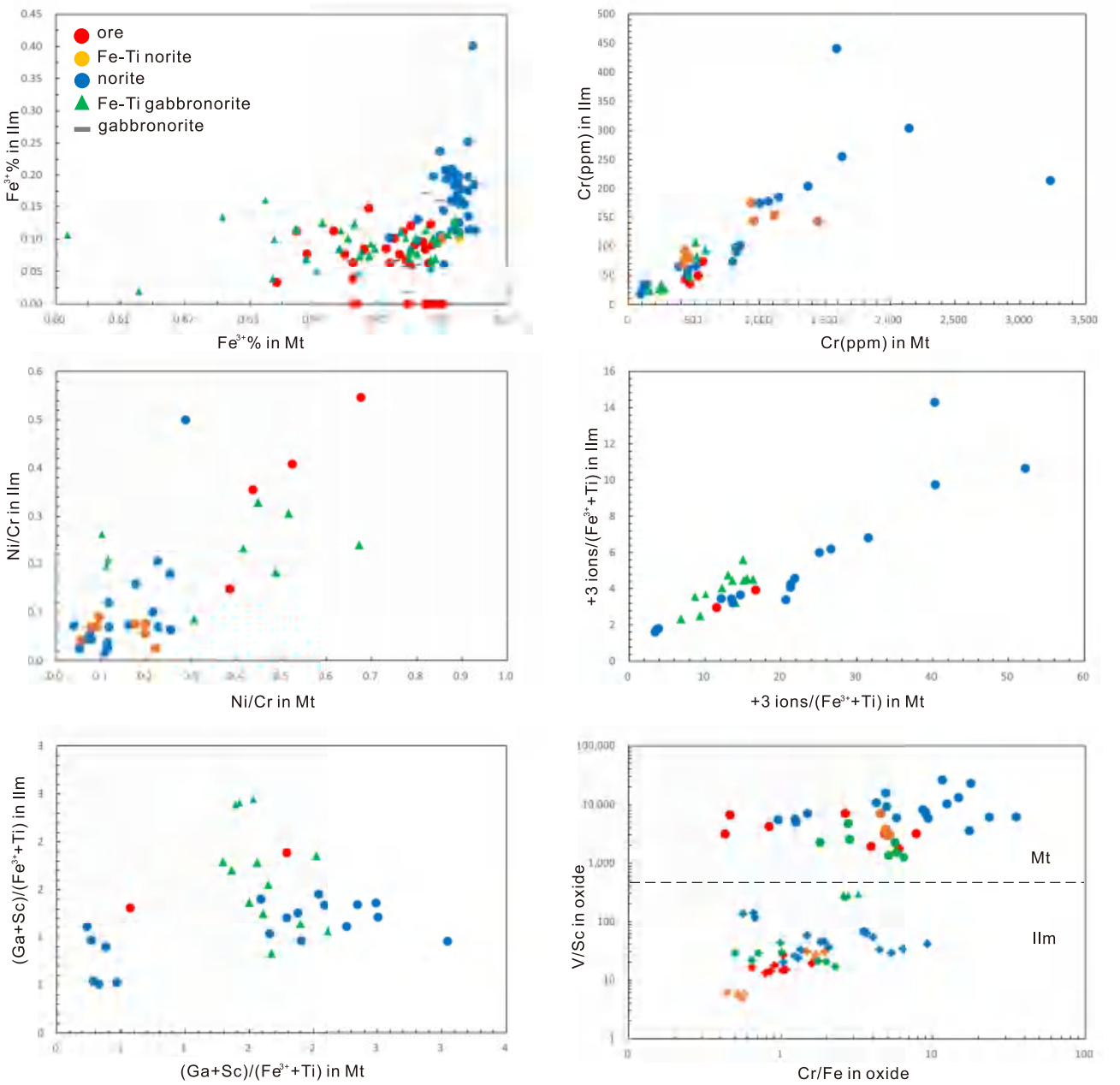

Fig. 7 Bi-elemental variation diagrams of magnetite and ilmenite from various ores or rocks

solid-solution end-members enriched in magnetite or ilmenite (Lindsley 2018). The subsolidus diffusion reactions cease at approximately 500–650 °C. Low-valence, small-radius ions like Fe^{2+} and Mn^{2+} diffuse in magnetite at rates significantly higher than in ilmenite. When Fe^{2+} diffuses into ilmenite via interstitialcy diffusion and co-precipitates with Fe^{3+}, it forms magnetite exsolution; conversely, the magnetite–ulvöspinel solid solution forms ilmenite exsolution due to the loss of Fe^{2+} (Tan et al. 2016, 2019; Arguin et al. 2018).

This process indicates that the diffusion coefficients of Fe^{2+}, Fe^{3+}, and Ti^{4+} in iron–titanium oxides under varying temperatures and oxygen fugacities are critical factors limiting the extent of reactions and the exsolution of iron–titanium oxides (Sievwright et al. 2020). Element diffusion in these oxides is influenced not only by ionic radius, valence, and ionization energy but also by factors such as rock temperature, oxygen fugacity, cooling history, mineral chemistry, and compositional gradients (Orman and Crispin 2010; Dohmen et al. 2019). The primary diffusion mechanisms of elements in iron–titanium oxide solid solutions are interstitialcy diffusion and vacancy diffusion. Interstitialcy diffusion occurs when smaller, low-valence ions (e.g., Fe^{2+}, Mn^{2+},

Zn^{2+}) move through the interstitial sites within the crystal lattice, causing minimal lattice distortion and thus being more efficient. Vacancy diffusion involves higher valence ions (e.g., V^{5+}, Sc, Ga, Co, Cr) moving into vacant lattice sites, and this process is more constrained by temperature and oxygen fugacity (Aragon 1979). In the Damiao deposit, ilmenite exhibits Fe-Mn striping, and the geochemical composition of magnetite is more uniform than that of the ilmenite, indicating that the diffusion rate of elements in ilmenite is significantly lower than in magnetite (Fig. 7). Diffusion rates of different elements in magnetite-ulvöspinel can differ by up to four orders of magnitude. The approximate order is:

$$\mathrm{Cr} < \mathrm{V} < \mathrm{Ti} < \mathrm{Al} < \mathrm{Sc} \approx \mathrm{Ga} \approx \mathrm{Zr} < \mathrm{Ni} < \mathrm{Zn} < \mathrm{Mn} < \mathrm{Mg} < \mathrm{Co} < \mathrm{Li} < \mathrm{Cu}$$

Thus, the elemental contents of Cu, Co, Mg, Mn, and Zn are highly susceptible to the effects of diffusion re-equilibration reactions, while elements such as Cr, Ti, Sc, and Ga have slower diffusion rates, largely preserving the original characteristics of magmatic crystallization evolution (Tanner et al. 2014).

In the magnetite–ulvöspinel and ilmenite–hematite solid solutions of the Damiao deposit, the correlations of divalent ion ratios (Mg + Mn + Zn)/Fe are poor, approximately presenting as straight lines with negative slopes (Fig. 7). This pattern confirms that elemental diffusion alters solid solution compositions due to competition among solid solution minerals for highly compatible elements. In contrast, the ratios of high-valence ions (Cr + Sc + Ga)/Fe^{3+} exhibit synchronous linear growth, reflecting the normal incorporation of compatible elements into minerals from Fe-Ti-P magma and the compositional evolution of the minerals (Fig. 7). Based on these observations, we conclude that Mg, Mn, and Zn are more inclined towards interstitialcy diffusion, while Cr, Sc, and Ga are more likely to undergo vacancy diffusion.

The diffusion re-equilibration of transition elements between iron–titanium oxides is affected not only by relative partition coefficients but also by the relative abundances of magnetite and ilmenite (Buddington and lindsley 1964; Charlier et al. 2015). The decoupling of geochemical characteristics of divalent ions in the two types of iron–titanium oxide solid solutions in the Damiao deposit confirms that elemental diffusion altering solid-solution compositions is widespread (Fig. 7). However, magnetite dominates the iron–titanium oxides in the Damiao deposit. When unit masses of Fe^{2+} and Ti^{4+} diffuse from magnetite into ilmenite, the change in ilmenite composition is significant, whereas the change in magnetite composition is almost negligible. From the perspective of chemical reaction mass balance, even if all the Fe^{3+} in the small amount of magmatically crystallized ilmenite–hematite solid solution in the Damiao deposit participates in the re-equilibration reaction, it can only account for minor proportion of the ilmenite exsolution in magnetite–ulvöspinel. Consequently, in the Damiao deposit, subsolidus re-equilibration reactions between magnetite and ilmenite solid solutions can at most be considered a supplementary mechanism for the oxidative exsolution of magnetite.

5.3 Solubility and crystallization processes of lithophile elements in Fe-Ti-P magma

In the Damiao deposit, exsolved zircon is observed at the edges of ilmenite, adjacent to altered clinopyroxene (Fig. 4). This suggests that the exsolution of zircon is likely the result of $Fe^{2+} \leftrightarrow Zr^{4+}$ exchange via diffusion between ilmenite and clinopyroxene. However, due to their valence states and ionic radii, Zr^{4+} and Si^{4+} have very slow diffusion rates in iron–titanium oxide solid solutions (Tanner et al. 2014; Tan et al. 2016). As a result, this reaction ultimately leads to the crystallization of zircon near the clinopyroxene end-member rather than within the ilmenite.

An alternative explanation for the presence of zircon exsolution in ilmenite is the dissolution–saturation process within the magma. However, the primary cause is likely related to the increase in Zr concentration in the magnetite caused by the exsolution of ilmenite, with late magmatic hydrothermal activity also playing a potential role (Charlier et al. 2017; Bingen et al. 2001). The solubility of elements in Fe-Ti-P magma is governed not only by temperature, pressure, and oxygen fugacity but also by the content and forms of iron–titanium oxides present. The forms and presence of iron–titanium oxides, such as magnetite and ilmenite, can especially influence solubility by providing specific nucleation sites or by sequestering certain elements, thereby affecting their availability in the magma (Tanner et al. 2014). This effect is particularly pronounced for siderophile elements such as Cr, Co, Ti, Mn, and Al. Zr^{4+} and Si^{4+} in magma do not display siderophile behavior, so they are not incorporated into the composition of iron–titanium oxide solid solutions (Morisset and Scoates 2008). Therefore, the exsolution of zircon in the Damiao deposit may result from increased concentrations of Zr^{4+} and Si^{4+} in the residual melt due to the crystallization of ilmenite–hematite solid solutions, leading to their saturation and subsequent precipitation. This also explains why zircon precipitates at the edges of ilmenite rather than at the center.

Although Al in Fe-Ti-P magma, like Zr, is not a siderophile element, it can occupy tetrahedral coordination sites in iron–titanium oxides, forming magnetite (Fe_3O_4)–pleonaste [$(Mg_X, Fe_{2-X})Al_2O_4$] solid solutions, or it can form corundum (Al_2O_3). Exsolved corundum within magnetite has been found in the Lac Doré deposit in Canada and the Panzhihua deposit in China (Arguin et al. 2018; Tan et al. 2016). Aluminum primarily exists in the form

of pleonaste, which can be categorized into blocky and lamellar types based on their structures and morphologies (Fig. 3). The blocky pleonaste is located at the edges of ilmenite, adjacent to magnetite and titanomagnetite, indicating that the crystallization of pleonaste is influenced by both ilmenite and magnetite. Pleonaste exsolution occurs at significantly higher temperatures compared to the formation of cloth-textured intergrowths of magnetite and ulvöspinel (Benavent et al. 2017). Therefore, the crystallization of pleonaste is likely due to Al saturation in the magma at eutectic temperature or Al saturation in titanomagnetite caused by the oxidation exsolution of ilmenite. Overall, this process involves concentration changes leading to Al saturation and subsequent crystallization. Due to its ionic radius and valence, Al has a very low diffusion rate in magnetite–titanomagnetite solid solutions. As ilmenite extends outward through oxidation exsolution, the pleonaste that originally crystallized outside the ilmenite becomes enveloped by ilmenite. In some ilmenite edges in the Damiao deposit, multiple pleonaste rings are observed, indicating that continuous oxidation exsolution of ilmenite led to multiple episodes of saturation and precipitation of pleonasste (Figs. 3, 5). Lamellar pleonaste, which grows along the < 100 > directions within magnetite, crosscuts lamellar ilmenite that grows along the < 111 > direction. This indicates that the exsolution of lamellar pleonaste occurred later than that of lamellar ilmenite, reflecting a sequential cooling history of the Damiao deposit, indicating that pleonaste exsolution in the Damiao deposit persisted from approximately 850 °C to around 500 °C, traversing the eutectic line of magnetite–pleonaste. This finding provides new evidence for studying the cooling history of the Damiao intrusion.

5.4 Cooling history of the damiao Fe-Ti-P oxide rocks and implications for the immiscible origin of nelsonitic melts

The cooling history of the Damiao complex can be constrained by the geological processes discussed in previous sections, namely, the redox reactions and subsolidus equilibrations among iron–titanium oxides or between these oxides and silicate minerals. The direction of each process, along with the temperature, pressure, and oxygen fugacity ranges within which the substances remain stable, can be determined by the Gibbs free energy of the corresponding chemical reactions:

$$\Delta G = \sum_{1}^{n} v_I^j \cdot \mu_I^j \leq 0 \tag{4}$$

where ν and μ represent the stoichiometric coefficients and chemical potentials, respectively. The chemical potential is calculated using:

$$\mu_I^j = \Delta H_{i,T_r,P_r}^{o,j} - T \cdot S_{i,T_r,P_r}^{o,j} + \int_{T_r}^{T} C_P \cdot dT - T \cdot \int_{T_r}^{T} \frac{C_P}{T} \cdot dT + \int_{P_r}^{P} V_{i,T,P}^{o,j} \cdot dP + R \cdot T \cdot \ln a_I^j \tag{5}$$

where ΔH^0 and S^0 are, respectively, the standard molar enthalpy and entropy of substance I under standard conditions (T_r, P_r), C_P and $V_{i,T,P}$ represent the heat capacity and molar volume of substance I at specific temperatures and pressures, respectively, and α denotes the activity of substance I. The standard-state thermodynamic parameters and activity data of iron–titanium oxides involved in these reactions are primarily referenced from the U.S. Geological Survey standards published in 1995, and the QUILF and WinMLgob databases and programs. These include standard molar enthalpy, entropy, heat capacity, and activity coefficients for various iron–titanium oxides (Andersen et al. 1993; Yavuz 2021). Experimental methods mainly involve phase equilibration and calorimetry to measure entropy, enthalpy, and heat capacity. The databases and computational programs encompass numerous thermodynamic models of iron–titanium oxide solid solutions accumulated over the years (Lindsley and Frost 1992; Andersen et al. 1993; Sauerzapf et al. 2008; Ghiorso and Evans 2008). Additionally, the entropy and enthalpy changes resulting from the structural transition of ilmenite–hematite solid solutions from R $\overline{3}$ C to R $\overline{3}$ with temperature are primarily referenced from Richardson et al. (2000). The thermal expansion and compression coefficients of iron–titanium oxides, derived from the least-squares fitting results by Wechsler and Prewitt (1984), are essential for adjusting the volumes and activities of these oxides at varying temperatures and pressures. These adjustments are crucial for accurately calculating the Gibbs free energy and, consequently, for determining the cooling history of the Damiao deposit. Errors in temperature, pressure, oxygen fugacity, and chemical composition are incorporated into the Gibbs free energy calculations throughout the computational process.

This study primarily infers the cooling history of the intrusion using mineral compositions from Damiao Fe-Ti-P ores, nelsonites, and gabbronorites. The main evidence includes: (1) the iron–titanium oxides in the Damiao deposit are predominantly magnetite, with exsolved blocky, lamellar, and cloth-textured ilmenite exhibiting relatively uniform compositions (Fig. 8); (2) the geochemical characteristics of magnetite, ilmenite, and clinopyroxene in the Damiao intrusion indicate elemental diffusion and compositional equilibration processes among iron–titanium oxides and

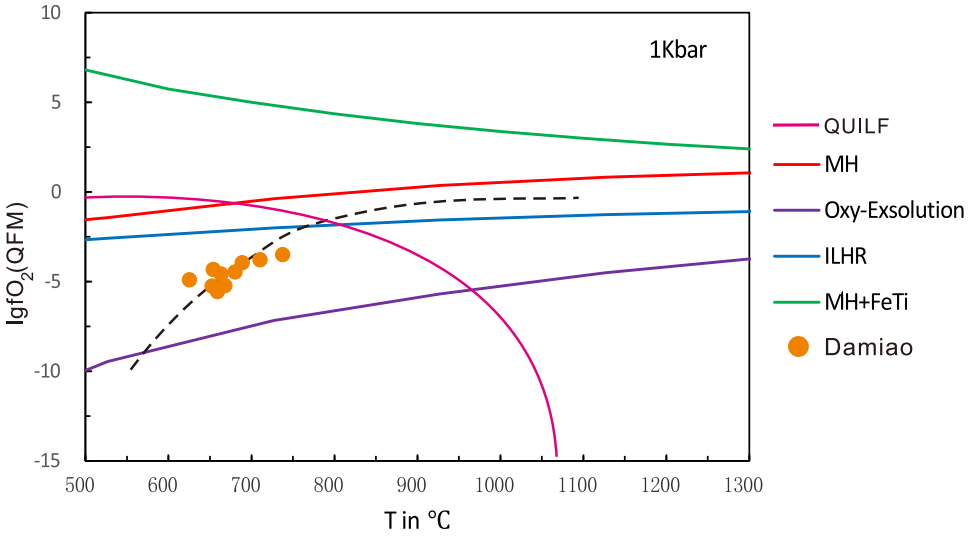

Fig. 8 Oxygen fugacity–temperature diagram showing the inferred cooling trend for Fe-Ti oxides in the Damiao deposit. MH + FeTi is based on the QUILF program calculations of the redox reactions between magnetite and hematite, and an inter-oxide re-equilibration between spinel and ilmenite–hematite. $_{ss}$*ILHR* ilmenite–hematite-rutile equilibrium, *MH* hematite–magnetite buffer, *oxy-exsolution* ulvöspinel–magnetite–ilmenite equilibrium, *QUILF* quartz–ulvöspinel–ilmenite–fayalite equilibrium

between these oxides and silicate minerals (Fig. 6, 7, 8); and (3) the oxygen fugacity–temperature evolution curve calculated using magnetite and ilmenite compositions from Damiao via the QUILF program approximately coincides with the Usp = 30% isopleth (Fig. 8). This is very close to the composition of titanomagnetite estimated from the exsolution proportions and in situ compositions of ilmenite. Therefore, the intersection points of the oxygen fugacity–temperature evolution curve of the Damiao deposit with the thermodynamic equation curves in the Fe-Ti-Si system approximately reflect the temperature and oxygen fugacity ranges of the corresponding processes occurring in the magma chamber. Meanwhile, the exsolution temperatures of pleonaste can also be determined based on the solvus lines of the Fe_2TiO_4–Fe_3O_4, $FeTiO_3$–Fe_2O_3, and Fe_3O_4–$FeAl_2O_4$ solid solutions.

The geochemical characteristics of iron–titanium oxides in the Damiao deposit confirm that the initial conditions of the Fe-Ti-P magma were relatively reducing. The evolution curve of these oxides lies below the magnetite–hematite (MH) buffer curve, indicating the cooling history was dominated by magnetite (Fig. 8). Subsolidus elemental equilibration between magnetite and ilmenite is primarily achieved through the diffusion of Fe and Ti. Although thermodynamic equations suggest this reaction is independent of oxygen fugacity, the chemical compositions of oxide mineral assemblages (e.g., magnetite–hematite and ulvöspinel–ilmenite buffers) are constrained by oxygen fugacity. At low temperatures, the solubility of Ti in magnetite decreases, and the elemental equilibration between iron–titanium oxides tends to form relatively pure magnetite and ilmenite end-members (Evans et al. 2006; Tan et al. 2016). The thermodynamic curve of this reaction approximates the MH buffer curve. At high temperatures, the solubility of Ti in magnetite–ulvöspinel solid solutions increases, and the influence of oxygen fugacity on this reaction gradually diminishes, eventually becoming negligible above 1000 °C (Frost 1991).

Calculations of Damiao oxide composition using the QUILF program indicate that elemental diffusion between iron–titanium oxides begins to occur at temperatures of 700–800 °C and oxygen fugacity conditions from quartz–fayalite–magnetite (QFM) to QFM–1 (Fig. 8). These conditions are close to those of the oxidation process of ulvöspinel. Once oxidation exsolution begins, the insoluble Ti in magnetite finds suitable positions without needing to diffuse out of the magnetite solid solution. Therefore, the compositions of magnetite–ulvöspinel and exsolved ilmenite can approximately indicate the temperature and oxygen fugacity conditions where elemental diffusion processes terminate. However, due to the high valence and large ionic radius of Ti^{4+}, its diffusion effect in magnetite is minimal (Tanner et al. 2014). When the temperature drops below 600 °C, the diffusion of Ti ions nearly ceases, making it unrealistic to calculate the exact conditions for the termination of elemental diffusion based solely on oxide compositions.

In the Damiao deposit, oxidation of magnetite leads to significant differences in the compositions and structures of ilmenite exsolutions (Fig. 8). By estimating the composition of titanomagnetite and its crystallization temperature (approximately 800–850 °C) through mass balance using the compositions of magnetite and ilmenite exsolutions, we find that continuous crystallization of iron–titanium oxides causes the magma's temperature to gradually decrease. Elemental equilibrations occur between magnetite and ilmenite, followed by oxidation exsolution of ulvöspinel to form ilmenite due to increased oxygen fugacity. Blocky and lamellar ilmenite form above the solid-solution solvus at temperatures around 700 °C, while cloth-textured ilmenite forms below the solvus at temperatures around 530 °C

(Fig. 8). Various factors might account for the changes in oxygen fugacity of the Fe-Ti-P magma in Damiao. One possibility is the assimilation and contamination of wall rocks, enriching the magma with CO_2, H_2S, and H_2O, which could serve as oxygen sources. Recent studies on magmatic melt inclusions have supported this hypothesis (Iacono-Marziano 2020). Another possibility is the mixing of magmas with different degrees of evolution or varying oxygen fugacities (Cottrell et al. 2021).

The main mineral assemblage of the Damiao deposit consists of iron–titanium oxides, olivine, and clinopyroxene. Therefore, the elemental equilibration (QUILF) and redox reactions (QFM) between iron–titanium oxides and silicate minerals need to be incorporated into the evolution history calculations. The elemental equilibration in the QUILF thermodynamic equations does not directly involve oxygen. However, the compositions of iron–titanium oxide and olivine solid solutions are influenced by changes in the magma's oxygen fugacity. Higher oxygen fugacity leads to the formation of more oxidized mineral phases, such as magnetite, hematite, and forsterite end-members, while lower oxygen fugacity favors the formation of reduced phases. At high temperatures, the influence of oxygen fugacity on the elemental equilibration is minimal, and the reaction terminates when temperatures exceed olivine's crystallization temperature (Pang et al. 2008; Arguin et al. 2018). At low temperatures, the solubility of Ti in titanomagnetite decreases, leading to reduced ulvöspinel activity and increased magnetite activity. The reaction between iron–titanium oxides and SiO_2 in the magma gradually shifts from an elemental equilibration to a redox reaction (QFM). Calculations indicate that iron–titanium oxides react with SiO_2 in the magma to form olivine at around 700–800 °C (Fig. 8).

The oxide–apatite gabbronorites in the Damiao deposit primarily outcrop as veins or pseudo-layers, with iron–titanium oxides uniformly distributed among silicate interstitial phases, displaying cumulate textures (He et al. 2016, 2019), indicating that Fe-Ti oxide crystallization occurred concurrently with or slightly later than that of silicate minerals. Oxygen fugacity during the crystallization of oxide–apatite gabbronorites was significantly higher than during the crystallization of Fe-Ti-P ores, based on the Fe^{3+} content and V/Sc ratio of iron–titanium oxides. These factors provide constraints on the genesis of the Damiao deposit. The Damiao deposit primarily formed from ferrodioritic magmas (Chen et al. 2013; He et al. 2016). The oxide–apatite gabbronorite resulted from Fe-Ti-P-rich residual melts after plagioclase and pyroxene fractional crystallization from the ferrodioritic magma. This residual melt evolved into Fe-Ti-P-rich melts through immiscibility, eventually crystallizing to form oxide ores (Chen et al. 2013; He et al. 2016). Therefore, the oxide–apatite gabbronorite and Fe-Ti-P ores can reflect changes in the parent magma's composition and oxygen fugacity conditions before and after immiscibility. Experimental study indicates that increasing magma oxygen fugacity can expand the compositional range over which immiscibility occurs, making Fe-rich melts more likely to separate from silicic magma (Hou et al. 2018). Combined with our calculations of the ferrodioritic magma's oxygen fugacity, this suggests that oxygen fugacity played a crucial role in the immiscibility process of Fe-Ti-P melts in the Damiao deposit.

6 Conclusion

The Damiao Fe-Ti-P deposit, located in the Damiao anorthosite complex in northeastern China, provides valuable insights into the formation processes of Fe-Ti oxide ores within mafic intrusions. Detailed petrographic observations and geochemical analyses conducted in this study reveal that the diverse ilmenite exsolution textures found in titanomagnetite arise from a complex interplay of magmatic events and subsolidus transformations. These textures, which include blocky, lamellar, and cloth-like forms, originated from various mechanisms operating under different temperature regimes and oxygen fugacity conditions. The primary mechanisms identified for the formation of these textures are magmatic oxidation events (oxy-exsolution) due to the oxidation of titanomagnetite, subsolidus re-equilibration between magnetite and ilmenite facilitated by elemental diffusion (notably of Fe, Ti, Cr, Co, and Ni), and exsolution induced by rapid cooling leading to lattice defects. Thermodynamic modeling using Gibbs free energy calculations and the QUILF program supports these findings, indicating that these exsolution textures formed above and below the solid solution solvus at varying oxygen fugacities. The variable oxygen fugacity, combined with the cooling trajectory of the ferrodioritic magma, played a crucial role in controlling the mineralogical and textural evolution of the deposit. Additional mineralogical transformations were observed, including the exsolution of zircon at ilmenite grain boundaries, which is attributed to the increased concentration of Zr due to the oxidation of titanomagnetite, rather than interactions with adjacent clinopyroxene. The formation of pleonaste is linked to the higher aluminum content in the solid solution, a result of ilmenite oxidation. These processes underscore the significant role of lithophile element saturation and dissolution processes in titanomagnetite, rather than elemental exchanges and subsolidus reactions in the evolution of the deposit's mineralogy. The reconstructed cooling history suggests that the oxygen fugacity of oxide–apatite gabbronorites was significantly higher than that of Fe-Ti-P ores, confirming that increasing oxygen fugacity during magma evolution promoted immiscibility, leading to the formation of nelsonitic melts and ultimately the development of Fe-Ti-P ores.

Acknowledgements We sincerely thank Wenqin Zheng and Xiang Li for their assistance in EPMA laboratory work and data processing.

Authors' contributions KW: Designed the research framework and study objectives. Conducted detailed petrographic observations of the Damiao Fe-Ti-P deposit, focusing on the diverse ilmenite exsolution textures within titanomagnetite. Performed electron microprobe analyses to determine the geochemistry and mineralogy of the exsolutions. Drafted the initial manuscript, particularly sections on the formation mechanisms and implications of the exsolutions for the ore-forming process. HH: Assisted in the collection and analysis of geochemical data. Contributed to the thermodynamic modeling using Gibbs free energy calculations to understand the temperature and oxygen fugacity conditions under which the exsolutions formed. Participated in manuscript revisions, enhancing the discussion on the physicochemical conditions and cooling history of the deposit. WS: Provided the geological context of the Damiao deposit, including insights into the Proterozoic anorthosite complexes and mafic-ultramafic intrusions. Helped interpret the complex ilmenite exsolution textures and their relevance to the ore-forming processes.

Funding This work was funded by the National Natural Science Foundation of China (grant 42102094) and Natural Science Foundation of Hebei (Grant D2022402028).

Data availability Data and samples used in this study are available from the corresponding author upon reasonable request.

Declarations

Conflict of interest On behalf of all authors, the corresponding author states that there is no conflict of interest.

Consent for publication All authors have read and approved the final version of the manuscript and agree to its submission to Acta Geochimica.

References

Adak S et al (2021) Textural re-equilibration, hydrothermal alteration and element redistribution in Fe-Ti oxide pods, Singhbhum Shear Zone, eastern India. Geochemistry 81(1):125679

Andersen DJ et al (1993) QUILF: A pascal program to assess equilibria among Fe-Mg-Mn-Ti oxides, pyroxenes, olivine, and quartz. Comput Geoci 19(9):1333–1350

Aragon R (1979). Chemical equilibria and kinetics associated with reactions in the magnetite-ulvospinel system, Purdue University.

Arguin J-P et al (2018) An integrated model for ilmenite, Al-spinel, and corundum exsolutions in titanomagnetite from oxide-rich layers of the Lac Doré Complex (Québec, Canada). Minerals 8(11):476

Bhattacharjee C, Mondal SK (2021) Geochemistry of Fe-Ti oxide and sulfide minerals in gabbroic rocks and magnetitite of the Archean Mayurbhanj mafic complex (eastern India): Magma fractionation, thermometry and oxygen fugacity of re-equilibration, and implications for Ni-Cu mineralization. Ore Geol Rev 131:104005

Bingen B et al (2001) Ilmenite as a source for zirconium during high-grade metamorphism? Textural evidence from the Caledonides of Western Norway and implications for zircon geochronology. J Petrol 42(2):355–375

Buddington AF, Lindsley D (1964) Iron-titanium oxide minerals and synthetic equivalents. J Petrol 5(2):310–357

Buelens P et al (2024) Multi-stage evolution of the monzonitic Larvik Plutonic Complex (Oslo Rift, Norway) and its implications for the formation of the Kodal Fe-Ti-P (− REE) deposit. Lithos 484:107743

Carter PW, Ward MD (1993) Topographically directed nucleation of organic crystals on molecular single-crystal substrates. J Am Chem Soc 115(24):11521–11535

Charlier B et al (2015) Fe–Ti–V–P ore deposits associated with Proterozoic massif-type anorthosites and related rocks. Earth Sci Rev 141:56–81

Charlier B et al (2007) Ilmenite composition in the Tellnes Fe–Ti deposit, SW Norway: fractional crystallization, postcumulus evolution and ilmenite–zircon relation. Contrib Miner Petrol 154:119–134

Chen WT et al (2013) Differentiation of nelsonitic magmas in the formation of the~ 1.74 Ga Damiao Fe–Ti–P ore deposit, North China. Contrib Miner Petrol 165:1341–1362

Cottrell E et al (2021) Oxygen fugacity across tectonic settings In: Magma redox geochemistry 33–61

Dellefant F et al (2024) Ilmenite phase transformations in suevite from the Ries impact structure (Germany) record evolution in pressure, temperature, and oxygen fugacity conditions. Am Miner 109(6):1005–1023

Dohmen R et al (2019) Diffusion of Zr, Hf, Nb and Ta in rutile: effects of temperature, oxygen fugacity, and doping level, and relation to rutile point defect chemistry. Phys Chem Miner 46:311–332

Evans BW et al (2006) Experimental determination of coexisting iron–titanium oxides in the systems FeTiAlO, FeTiAlMgO, FeTiAlMnO, and FeTiAlMgMnO at 800 and 900 °C, 1–4 kbar, and relatively high oxygen fugacity. Contrib Miner Petrol 152(2):149–167.

Frost BR (1991) Magnetic petrology; factors that control the occurrence of magnetite in crustal rocks. Rev Mineral Geochem 25(1):489–509

Gao W et al (2019) Nanoscale study of titanomagnetite from the Panzhihua Layered Intrusion, Southwest China: Multistage exsolutions record ore formation. Minerals 9(9):513

Gennaro E et al (2024) The kinetic effect induced by variable cooling rate on the crystal-chemistry of spinel in basaltic systems revealed by EPMA mapping. Am Miner 109(7):1171–1180

Ghiorso MS, Evans BW (2008) Thermodynamics of rhombohedral oxide solid solutions and a revision of the Fe-Ti two-oxide geothermometer and oxygen-barometer. Am J Sci 308(9):957–1039

Gorbatova E et al (2021) Solid-Phase Transformations of Titanomagnetite and Ilmenite during Oxidizing Roasting of Disseminated Titanomagnetite-Ilmenite Ore at the Medvedevskoe Deposit and Certain Geological Events (Southern Urals). Geol Ore Deposits 63(5):431–453

Harrison RJ, Putnis A (1997) Interaction between exsolution microstructures and magnetic properties of the magnetite-spinel solid solution. Am Miner 82(1–2):131–142

He H-L et al (2019) Lower crustal contribution to the magma formation of the Damiao massif-type anorthosite, North China Craton: Evidence from zircon Hf-O isotopes. Precambr Res 332:105396

He H-L et al (2016) Origin of nelsonite and Fe–Ti oxides ore of the Damiao anorthosite complex, NE China: Evidence from trace element geochemistry of apatite, plagioclase, magnetite and ilmenite. Ore Geol Rev 79:367–381

Hou T et al (2018) Immiscible hydrous Fe–Ca–P melt and the origin of iron oxide-apatite ore deposits. Nat Commun 9:1415

Iacono-Marziano G (2020) Interactions between magmas and host sedimentary rocks: A review of their implications in magmatic processes (magma evolution, gas emissions and ore processes)

Khedr MZ et al (2024) Mineralogy and Geochemistry of Titaniferous Iron Ores in El-Baroud Layered Gabbros: Fe-Ti Ore Genesis and Tectono-Metallogenetic Setting. Minerals 14(7):679

Lattard D (1995) Experimental evidence for the exsolution of ilmenite from titaniferous spinel. Am Miner 80(9–10):968–981

Lee JH et al (2022) Whole-rock geochemistry and mineral compositions of gabbroic rocks and the associated Fe–Ti (–V) oxide deposit in the Gonamsan intrusion, South Korea. Ore Geol Rev 148:105054

Li H et al (2014) Alteration of the Damiao anorthosite complex in the northern North China Craton: Implications for high-grade iron mineralization. Ore Geol Rev 57:574–588

Li LX et al (2019a) The link between an anorthosite complex and underlying olivine–Ti-magnetite-rich layered intrusion in Damiao, China: insights into magma chamber processes in the formation of Proterozoic massif-type anorthosites. Contrib Miner Petrol 174:1–21

Li L-X et al (2019b) Role of fluids in Fe–Ti–P mineralization of the Proterozoic Damiao anorthosite complex, China: Insights from baddeleyite–zircon relationships in ore and altered anorthosite. Ore Geol Rev 115:103186

Li L-X et al (2024a) Characterizing a new type of nelsonite recognized in the Damiao anorthosite complex, North China Craton, with implications for the genesis of giant magmatic Fe-Ti oxide deposits. Am Miner 109(1):184–197

Li Y et al (2024b) Prolonged evolution of syn-collisional progressive deformation of the Trans-North China Orogen: Structural and geochronological evidence from the Xiaoqinling region, central China. Gondwana Res 129:332–354

Lilova KI et al (2012) Thermodynamics of the magnetite-ulvöspinel (Fe_3O_4-Fe_2TiO_4) solid solution. Am Miner 97(8–9):1330–1338

Lindsley DH (2018) Oxide minerals: petrologic and magnetic significance, Walter de Gruyter GmbH & Co KG

Lindsley DH, Frost BR (1992) Equilibria among Fe-Ti oxides, pyroxenes, olivine, and quartz: Part I. Theory. Am Miner 77(9–10):987–1003

Liu J-F et al (2016) Late Paleoproterozoic tectonic setting of the northern margin of the North China Craton: Constraints from the geochronology and geochemistry of the mangerites in the Longhua and Jianping areas. Precambr Res 272:57–77

Liu R et al. (2024) Occurrence and enrichment mechanism of Co in Fe-Ti oxide deposits: A case study of the world-class Panzhihua deposit in SW China. Ore Geol Rev 106177

Liu W-M et al (2024) Genesis of the Devonian Habaqin ultramafic arc complex and associated low-grade Fe–Ti oxide mineralization in the northern North China Craton. Lithos 478:107625

Lusted K (2019) Textures of Titaniferous Magnetite within the Bushveld Igneous Complex South Africa, University of Pretoria (South Africa)

Morisset C-E, Scoates JS (2008) Origin of zircon rims around ilmenite in mafic plutonic rocks of Proterozoic anorthosite suites. Can Mineral 46(2):289–304

Noh J et al (2015) Magnetite Fe_3O_4 (111) surfaces: impact of defects on structure, stability, and electronic properties. Chem Mater 27(17):5856–5867

Otto T (2017) Texture development in titaniferous magnetites found in Layer 21 in the Bushveld Igneous Complex. University of Pretoria (South Africa), South Africa

Özdemir Ö, Dunlop DJ (1997) Effect of crystal defects and internal stress on the domain structure and magnetic properties of magnetite. Journal of Geophysical Research: Solid Earth 102(B9):20211–20224

Pang K-N et al (2008) Origin of Fe–Ti oxide ores in mafic intrusions: evidence from the Panzhihua intrusion, SW China. J Petrol 49(2):295–313

Pang K-N et al (2010) Flood basalt-related Fe–Ti oxide deposits in the Emeishan large igneous province, SW China. Lithos 119(1–2):123–136

Paton C et al (2011) Iolite: Freeware for the visualisation and processing of mass spectrometric data. J Anal at Spectrom 26(12):2508–2518

Pearce CI et al (2010) Fe site occupancy in magnetite-ulvospinel solid solutions: A new approach using X-ray magnetic circular dichroism. Am Miner 95(4):425–439

Pochon A et al (2024) Fluid inclusions in magmatic ilmenite record degassing in basic magmas. Communications Earth & Environment 5(1):626

Price GD (1981) Subsolidus phase relations in the titanomagnetite solid solution series. Am Miner 66(7–8):751–758

Qi L, Zhou M-F (2008) Platinum-group elemental and Sr–Nd–Os isotopic geochemistry of Permian Emeishan flood basalts in Guizhou Province, SW China. Chem Geol 248(1–2):83–103

Robie RA et al (1978) Thermodynamic properties of minerals and related substances at 298.15 K and 1 bar (105 pascals) pressure and at higher temperatures, Department of the Interior, US Geological Survey

Sauerzapf U et al (2008) The titanomagnetite–ilmenite equilibrium: new experimental data and thermo-oxybarometric application to the crystallization of basic to intermediate rocks. J Petrol 49(6):1161–1185

She Y-W et al (2014) The formation of P-rich Fe–Ti oxide ore layers in the Taihe layered intrusion, SW China: implications for magma-plumbing system process. Ore Geol Rev 57:539–559

Sievwright R et al (2020) Diffusion and partition coefficients of minor and trace elements in magnetite as a function of oxygen fugacity at 1150 ºC. Contrib Miner Petrol 175:1–21

Tan W et al (2022) Magnetite-rutile symplectite in ilmenite records magma hydration in layered intrusions. American Mineralogist: Journal of Earth and Planetary Materials 107(3):395–404

Tanner D et al (2014) Trace element stratigraphy of the Bellevue Core, Northern Bushveld: multiple magma injections obscured by diffusive processes. J Petrol 55(5):859–882

Teng X et al (2015) Devonian magmatism associated with arc-continent collision in the northern North China Craton: evidence from the Longwangmiao ultramafic intrusion in the Damiao area. J Asian Earth Sci 113:626–643

Van Orman JA, Crispin KL (2010) Diffusion in oxides. Rev Mineral Geochem 72(1):757–825

Villanova-de-Benavent C et al (2017) Fe–Ti (–V) oxide deposits of the Kunene Anorthosite Complex (SW Angola): mineralogy and thermo-oxybarometry. Minerals 7(12):246

Von Gruenewaldt G et al (1985) Exsolution features in titanomagnetites from massive magnetite layers and their host rocks of the upper zone, eastern Bushveld Complex. Econ Geol 80(4):1049–1061

Wan Y et al (2013) Is the Ordos block Archean or Paleoproterozoic in age? Implications for the Precambrian evolution of the North China Craton. Am J Sci 313(7):683–711

Wang M et al (2017) The origin of nelsonite constrained by melting experiment and melt inclusions in apatite: The Damiao anorthosite complex, North China Craton. Gondwana Res 42:163–176

Watanabe T, Funakubo H (2006) Controlled crystal growth of layered-perovskite thin films as an approach to study their basic properties. J Apply Phy 100(5).

Wechsler BA et al (1984) Crystal structure and cation distribution in titanomagnetites ($Fe_{3-x}Ti_xO_4$). Am Miner 69(7–8):754–770

Wei Y et al (2020) Geochemistry and iron isotope systematics of coexisting Fe-bearing minerals in magmatic FeTi deposits: a case

study of the Damiao titanomagnetite ore deposit, North China Craton. Gondwana Res 81:240–251
Yan Y-Q et al (2025) Carboniferous, not Paleoproterozoic, eclogite-facies metamorphism in the northern North China Craton as revealed by in situ garnet Lu-Hf and U-Pb geochronology. Earth Planet Sci Lett 653:119207
Yang Q-Y et al (2014) Late Paleoproterozoic charnockite suite within post-collisional setting from the North China Craton: petrology, geochemistry, zircon U-Pb geochronology and Lu–Hf isotopes. Lithos 208:34–52
Yavuz F (2021) WinMIgob: A Windows program for magnetite-ilmenite geothermometer and oxygen barometer. J Geosci 66(1):51–70
Zhai M, Santosh M (2013) Metallogeny of the North China Craton: link with secular changes in the evolving Earth. Gondwana Res 24(1):275–297
Zhang Z et al (2025) Distribution, occurrence and enrichment mechanism of Co in Fe-Ti oxide deposits: An example from the giant Hongge deposit, SW China. Ore Geol Rev 106465
Zhao T-P et al (2009) Geochemical and Nd–Hf isotopic constraints on the origin of the~ 1.74-Ga Damiao anorthosite complex, North China Craton. Lithos 113(3–4):673–690